Science Advances
AAAS

advances.sciencemag.org/cgi/content/full/6/51/eabd6798/DC1

Supplementary Materials for

Calmodulin acts as a state-dependent switch to control a cardiac potassium channel opening

Po Wei Kang, Annie M. Westerlund, Jingyi Shi, Kelli McFarland White, Alex K. Dou, Amy H. Cui, Jonathan R. Silva, Lucie Delemotte*, Jianmin Cui*

*Corresponding author: jcui@wustl.edu (J.C.); lucie.delemotte@scilifelab.se (L.D.)

Published 11 December 2020, *Sci. Adv.* **6**, eabd6798 (2020)
DOI: 10.1126/sciadv.abd6798

This PDF file includes:

Supplementary Materials

Supplementary Figure S1.

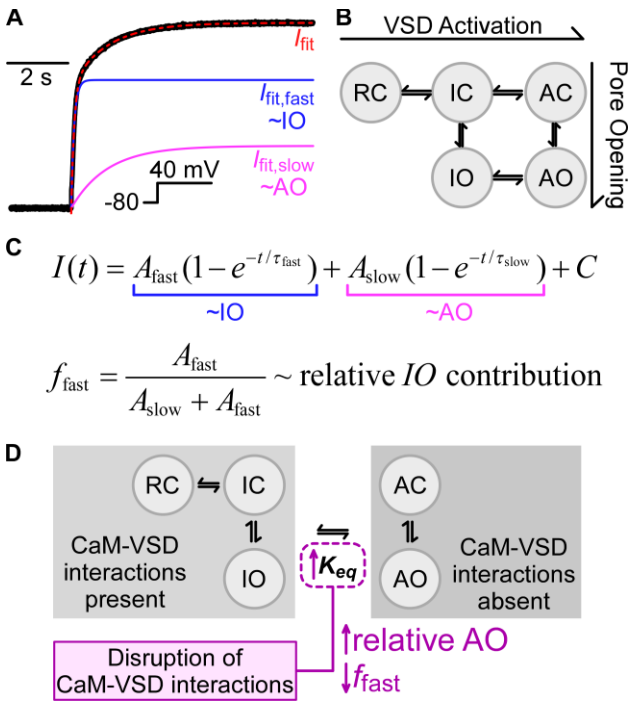

Supplementary Figure S1. Cartoon of the effect of disrupted CaM-VSD interactions on KCNQ1 bi-exponential current activation. Related to Main Figures 1, 2, and 4. **(A)** Exemplar current activation kinetics fit for KCNQ1-WT at +40 mV depolarization. **(B)** Two-open state gating model for KCNQ1. Horizontal transitions correspond to VSD activation and vertical transitions correspond to pore opening. RC: Resting-Closed, IC: Intermediate-Closed, IO: Intermediate-Open, AC: Activated-Closed, AO: Activated-Open. **(C)** Bi-exponential function used to fit the current kinetics, with the fast and slow components approximating IO (blue) and AO (magenta), respectively. The fraction of fast current component approximates relative IO contribution to the total current. **(D)** Proposed model of disrupting CaM-VSD interactions on KCNQ1. CaM-VSD interactions are favored in the RC, IC, IO states. Loss of CaM-VSD interactions destabilizes the RC, IC, and IO states, leading to enhanced AO state occupancy and manifesting as an increase in the relative AO state contribution (reduced f_{fast}). Please see Main Fig. 6E and main text for further results.

Supplementary Figure S2.

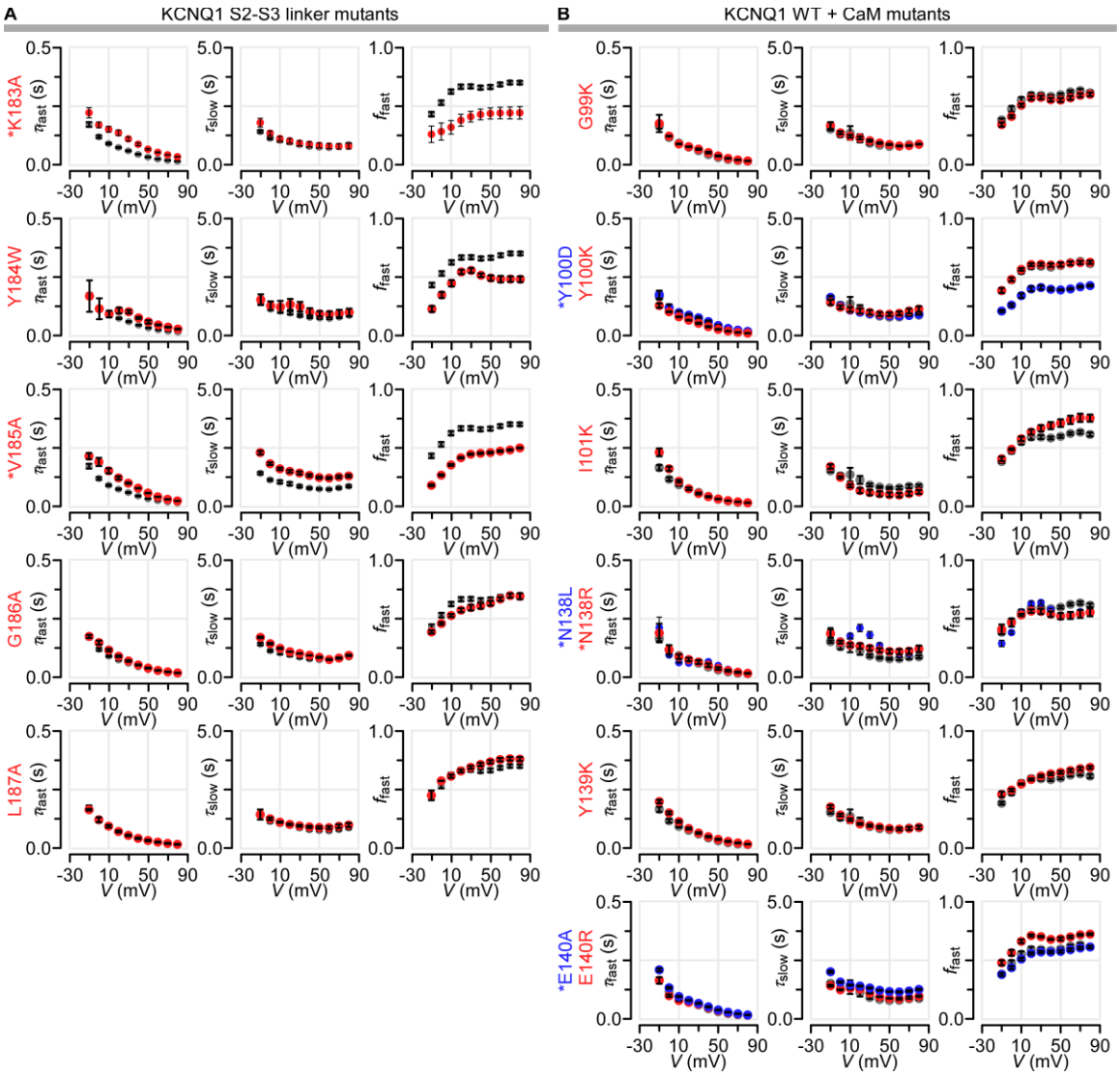

Supplementary Figure S2. Additional bi-exponential fits for current activation of several KCNQ1 mutants and KCNQ1 WT + CaM mutant. Related to Main Figures 1 and 2. (A-B) Each row shows the average bi-exponential fit parameters (fast time constant, slow time constant, fraction of fast current component) for S2-S3 linker mutants (panel A) and Q1 WT + CaM mutants (panel B). In all plots, grey corresponds to fitted parameters for Q1 WT + endogenous CaM WT (panel A) and Q1 WT + exogenous CaM WT (panel b). Red and blue correspond to the labeled mutants (see y-labels). Stars indicate mutants with statistically significant shifted $V_{1/2}$ compared to the corresponding WT (Main Figs. 1 and 2).

Supplementary Figure S3.

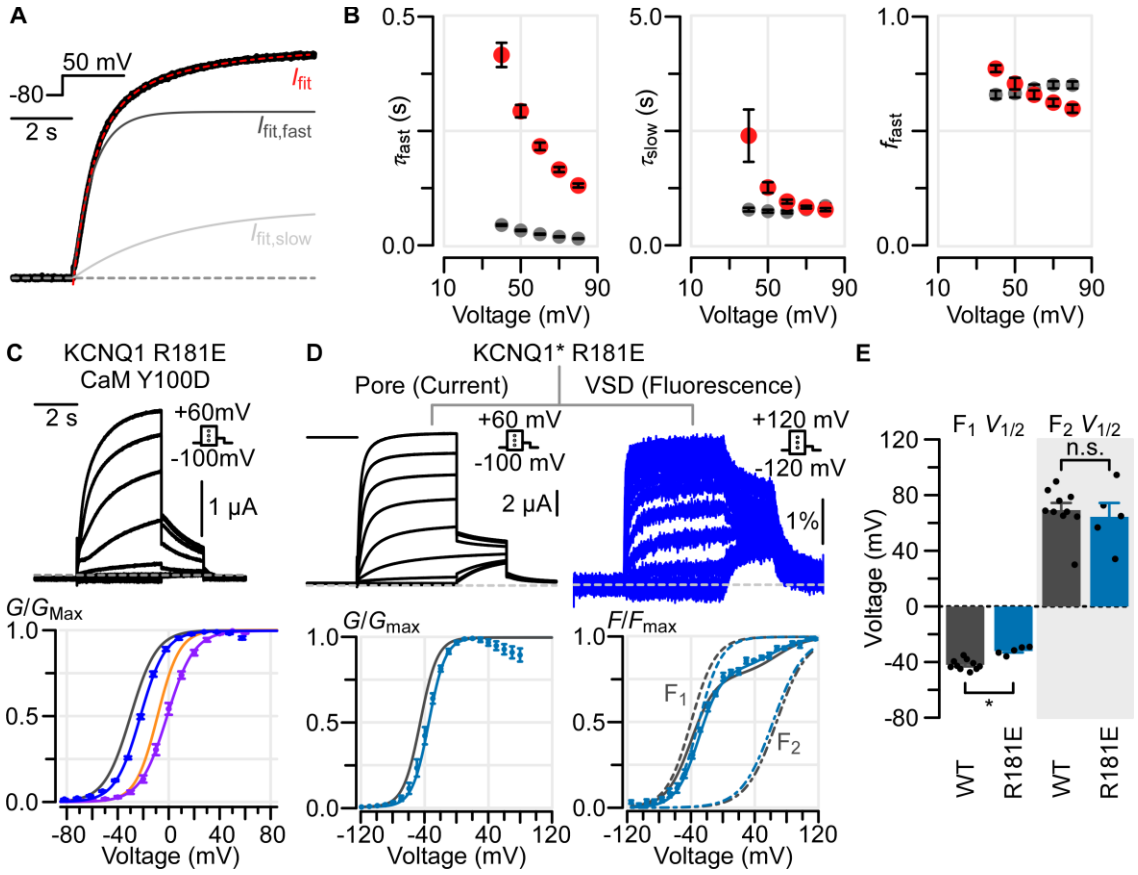

Supplementary Figure S3. Additional electrophysiology experiments for KCNQ1 R181E mutants. Related to Main Figures 1, 2, and 4. (A) Exemplar current activation kinetics fit for Q1-R181E at +50 mV depolarization. **(B)** Average bi-exponential kinetics fit parameters for Q1-WT (grey) and Q1-R181E (red, *n* = 5). Error bars are SEM. **(C)** Top: exemplar currents for Q1-R181E co-expressed with CaM-Y100D mutant. Bottom: average G-V relationships for Q1-WT + endogenous CaM-WT (grey); Q1-WT + exogeneous CaM-Y100D (blue); Q1-R181E + endogenous CaM-WT (orange); Q1-R181E + exogeneous CaM-Y100D (purple). CaM-Y100D induces a depolarizing shift of the G-V curves of the Q1-R181E mutant similar to the WT shift (Q1-R181E $V_{1/2}$=-8.74±1.48 mV, Q1-R181E + CaM-Y100D $V_{1/2}$ = -3.84±0.61 mV, *p*-value < 0.01, two sample T test assuming unequal variance). **(D)** VCF recordings for Q1*-R181E mutant. Top shows exemplar currents/fluorescence recordings and bottom shows the average

G-V/F-V fits. Grey indicates Q1*-WT and blue indicates Q1*-R181E. **(E)** Population $V_{1/2}$ of the double Boltzmann fits (F_1 and F_2) for Q1*-psWT and Q1*-R181E. Q1*-R181E demonstrates a significant shift in the F_1-V relationship ($p = 0.00015$) compared to Q1*-WT, indicating the voltage-dependence of VSD activation is altered by the R181E mutation. Error bars are SEM.

Supplementary Figure S4.

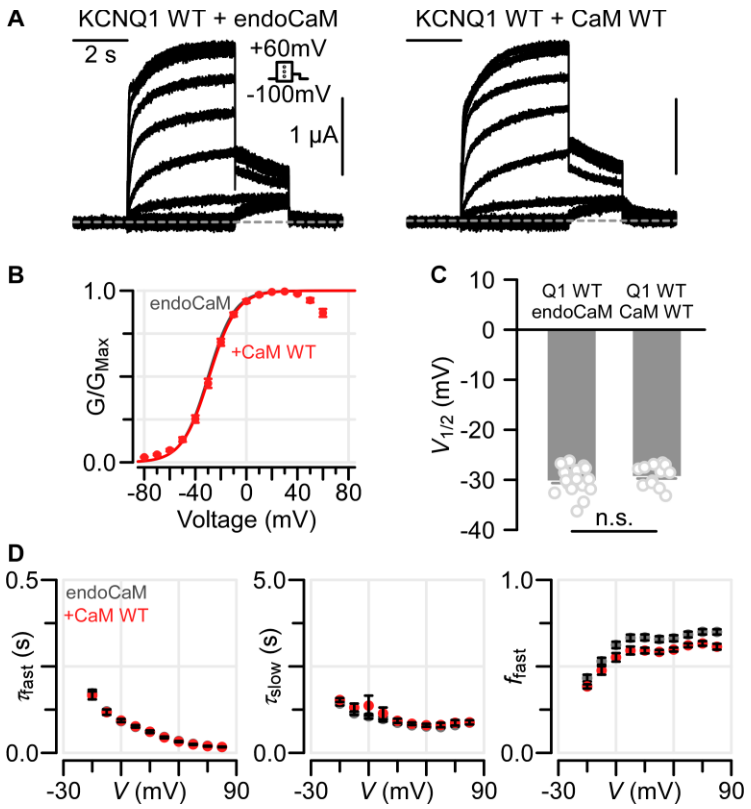

Supplementary Figure S4. Comparison of KCNQ1 WT current supplied with endogenous *Xenopus* CaM or over-expressed human CaM. Related to Main Figure 2. (A) Exemplar KCNQ1 currents obtained on the same day with endogenous CaM (left) and exogeneous human CaM WT (right). **(B)** Average G-V curves for KCNQ1 supplied with endogenous CaM (grey) and CaM WT co-expression (red, n = 12). **(C)** $V_{1/2}$ measured from KCNQ1 supplied with endogenous CaM (dataset in Main Figure 1) and CaM WT co-expression (dataset in Main Figure 2) are not significantly different (p = 0.32, two-sample T test assuming unequal variances). **(D)** Bi-exponential current kinetics analysis between KCNQ1 current with endogenous CaM (grey, n = 10) and CaM WT co-expression (red, n = 11). Error bars are SEM.

Supplementary Figure S5.

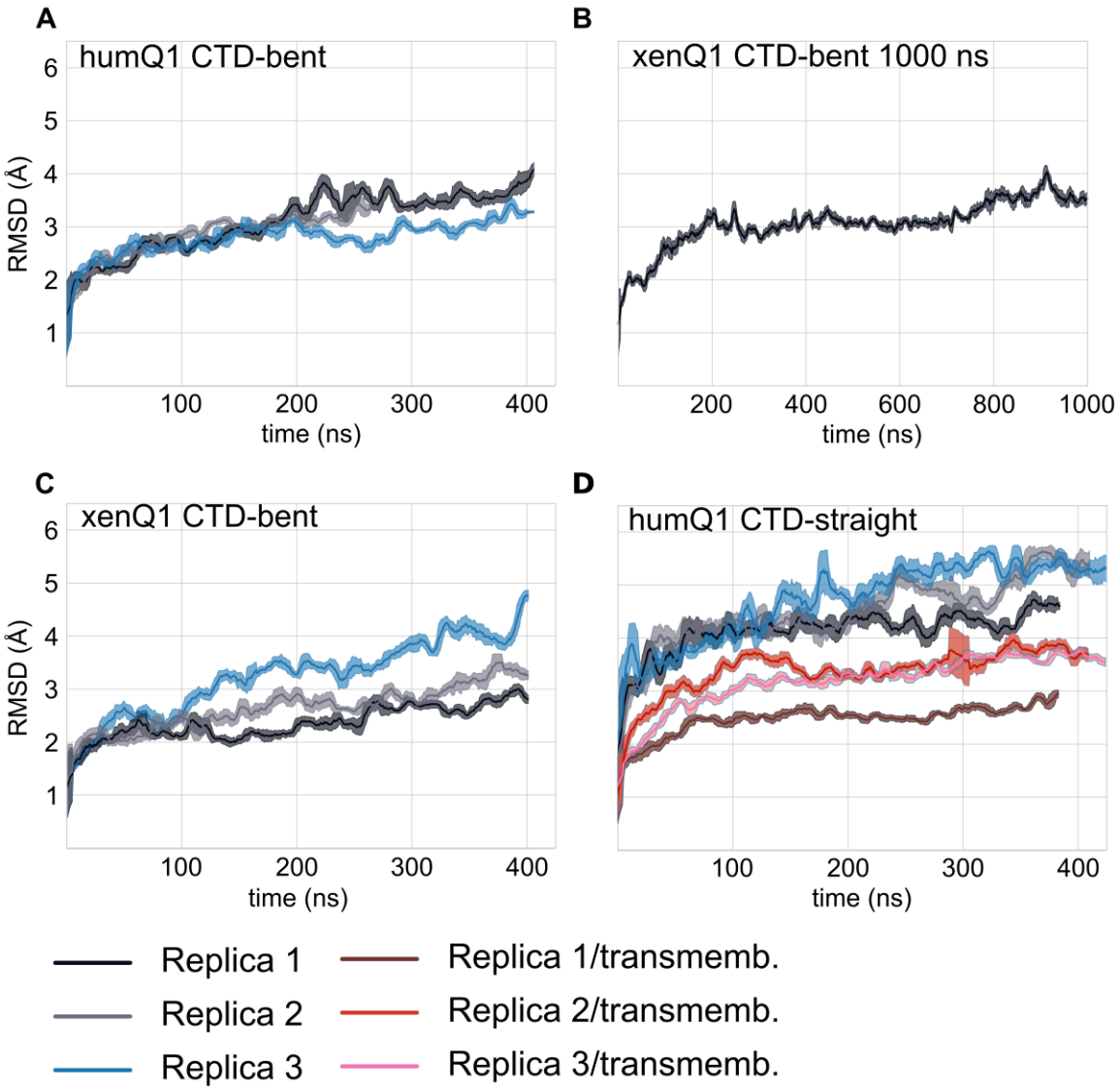

Supplementary Figure S5. RMSDs of molecular dynamics simulations of the human and *Xenopus* KCNQ1/CaM structures. Related to Main Figures 2, 3, and 5. RMSD along time for the **(A)** human KCNQ1/CaM CTD-bent simulations, **(B-C)** *Xenopus* KCNQ1/CaM CTD-bent control simulations and **(D)** human KCNQ1/CaM CTD-straight simulations with PIP_2. The RMSDs of the transmembrane region in the KCNQ1/CaM CTD-straight simulations highlight that the largest deviations occur in the intracellular domains. The RMSD time series are locally smoothed with an average filter with window size 9. Shaded regions show the local standard deviation.

Supplementary Figure S6.

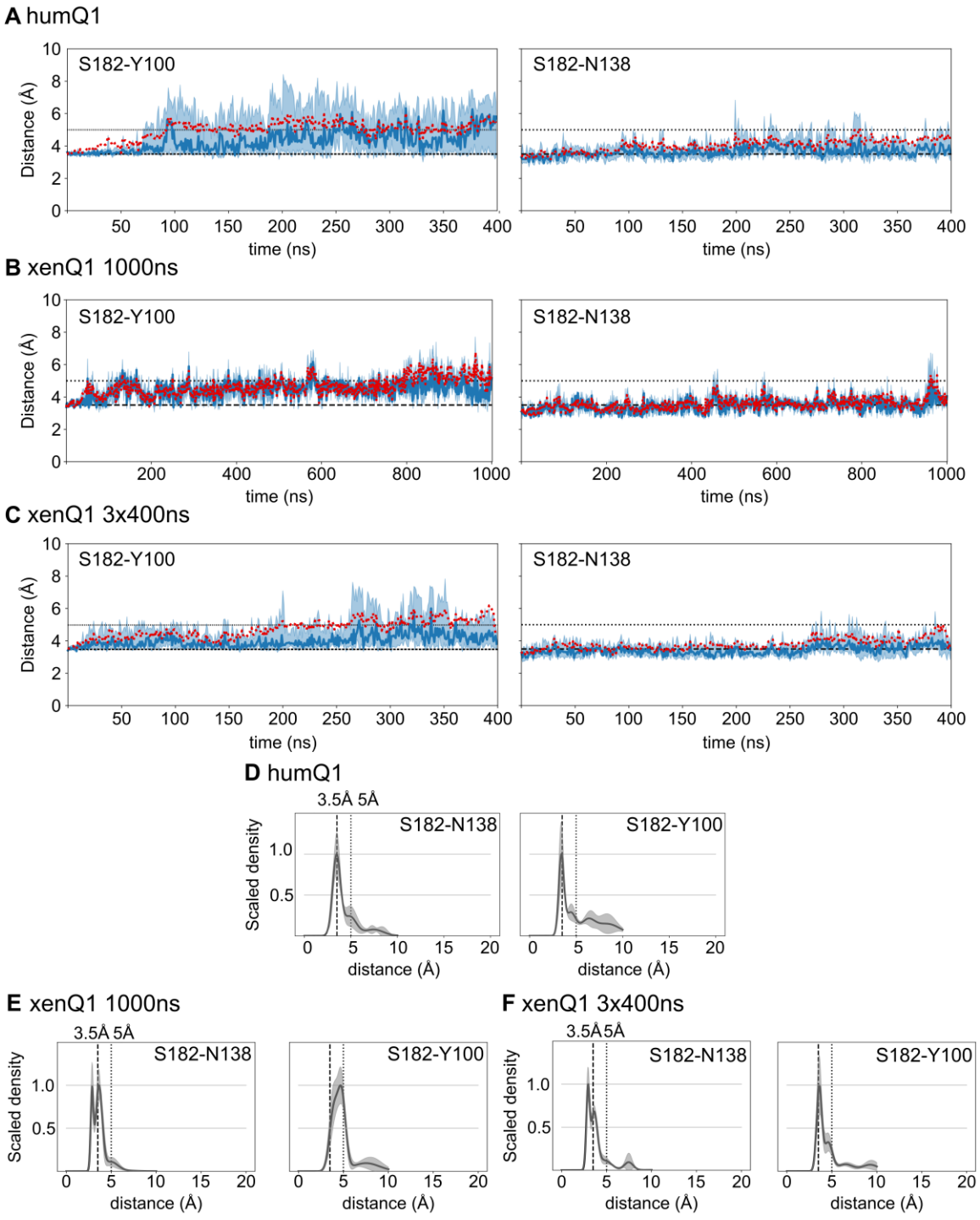

Supplementary Figure S6. Interaction distances between residues in the S2-S3 linker and CaM. Related to Main Figure 2. (A-C) Time series of interaction distances

showing median (blue line), mean (red dots), as well as the 25th and 75th percentiles (shaded). Statistics are obtained from all subunit trajectories. **(A)** human Q1 simulations (3x4=12 time series), **(B)** xenQ1 1000ns simulation (1x4=4 time series) and **(C)** xenQ1 3x400ns simulations (3x4=12 time series). **(D-F)** Scaled distance densities between selected residue pairs at the CaM/S2-S3 linker interface, calculated from **(D)** human Q1, **(E)** xenQ1 1000ns and **(F)** xenQ1 3x400ns KCNQ1/CaM CTD-bent simulations. Average and SEM are calculated over subunits.

Supplementary Figure S7.

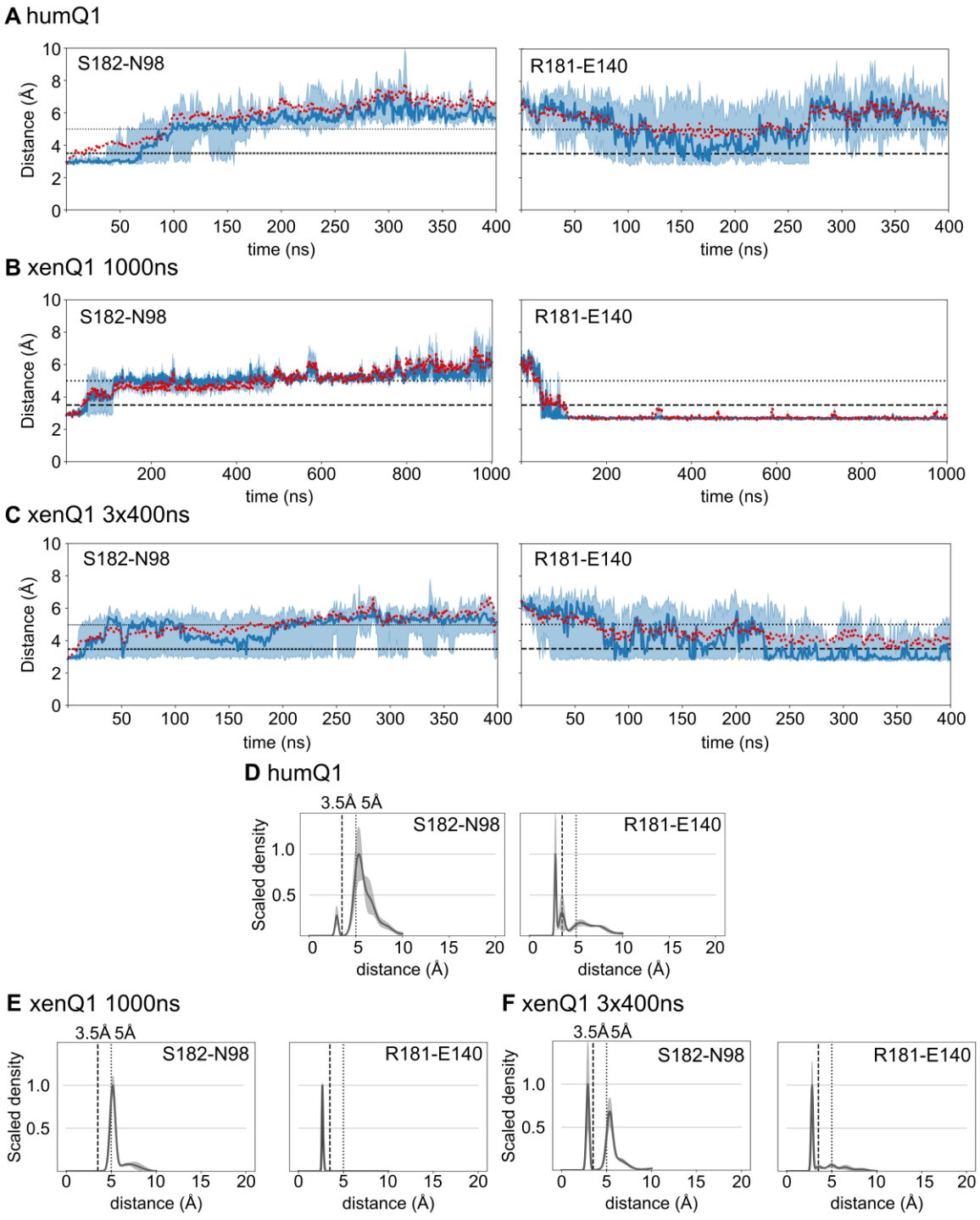

Supplementary Figure S7. Additional interaction distances between residues in the S2-S3 linker and CaM. Related to Main Figure 2. (A-C) Time series of interaction distances showing median (blue line), mean (red dots), as well as the 25th and 75th

percentiles (shaded). Statistics are obtained from all subunit trajectories. **(A)** human Q1 simulations (3x4=12 time series), **(B)** xenQ1 1000ns simulation (1x4=4 time series) and **(C)** xenQ1 3x400ns simulations (3x4=12 time series). **(D-F)** Scaled distance densities between selected residue pairs at the CaM/S2-S3 linker interface, calculated from **(D)** human Q1, **(E)** xenQ1 1000ns and **(F)** xenQ1 3x400ns KCNQ1/CaM CTD-bent simulations. Average and SEM are calculated over subunits.

Supplementary Figure S8.

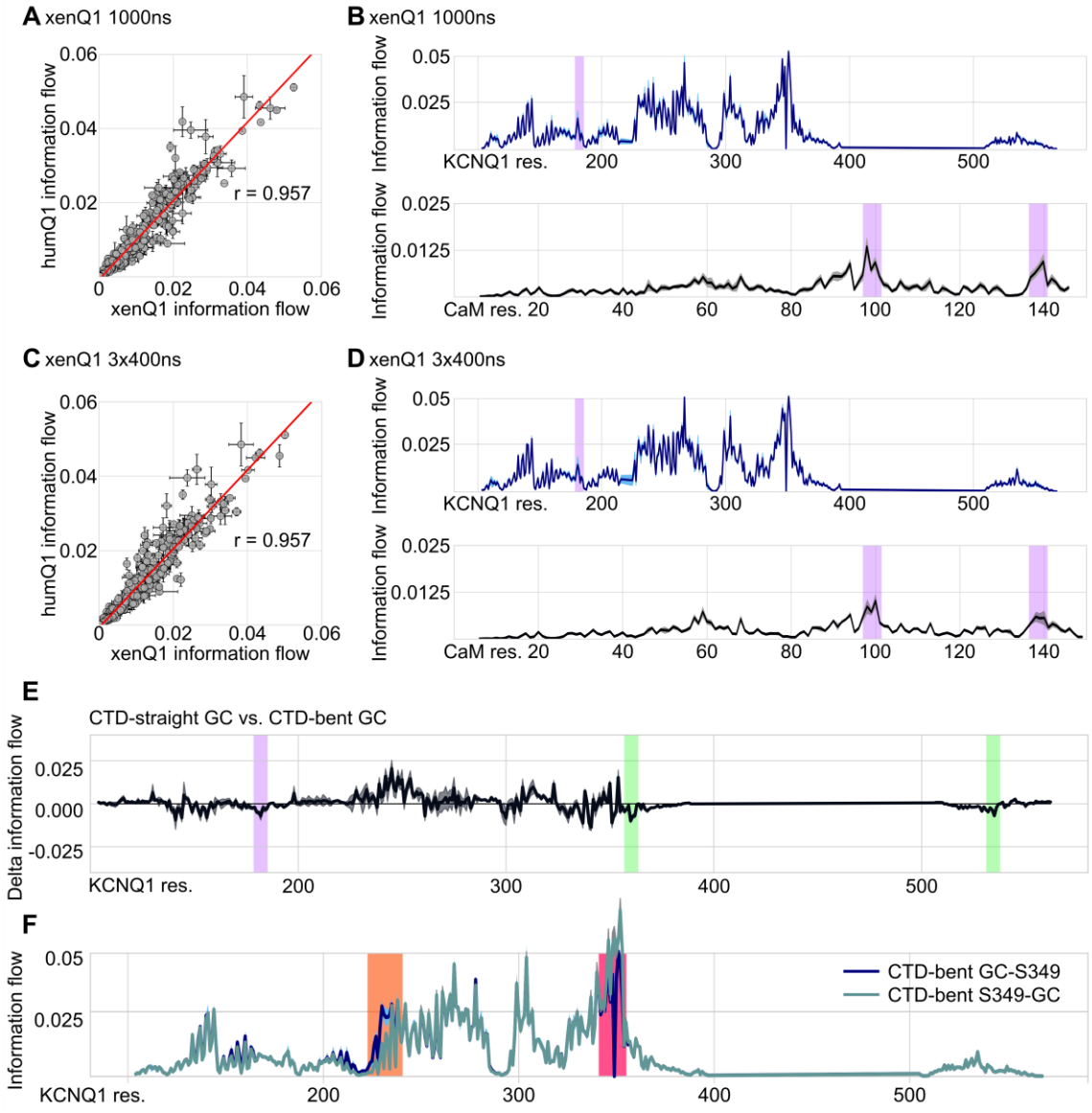

Supplementary Figure S8. Validation of network analysis. Related to Main Figure 3. (A) Correlation plot between the human KCNQ1/CaM CTD-bent and 1000ns *Xenopus* simulation gating charges-S349 information flows. **(B)** Information flow profiles of KCNQ1 and CaM (source: gating charges, sink: S349) in the 1000ns *Xenopus* simulation. **(C)** Correlation plot between the human KCNQ1/CaM CTD-bent and 3x400ns *Xenopus* simulations gating charges-S349 information flows. **(D)** Information flow profiles of KCNQ1 and CaM (source: gating charges, sink: S349) in the 3x400ns

Xenopus simulations. **(E)** Δinformation flow (source: gating charges, sink: S349), comparing the human KCNQ1/CaM simulations of CTD-straight and CTD-bent conformations. The profile averages and standard deviation (light blue) in (B, D) and gray in (E), are calculated across subunits. Human numbering is used for both human and *Xenopus* simulations for consistency. **(F)** Information flow profile obtained after reversing the sources and sinks (petrol) compared to the original CTD-bent Q1 profile. The gating charge (CG) sinks were divided into the four subunits prior to information flow averaging. The profiles only differ notably at the GC (orange) and at the original sink residue S349 (cerise).

Supplementary Figure S9.

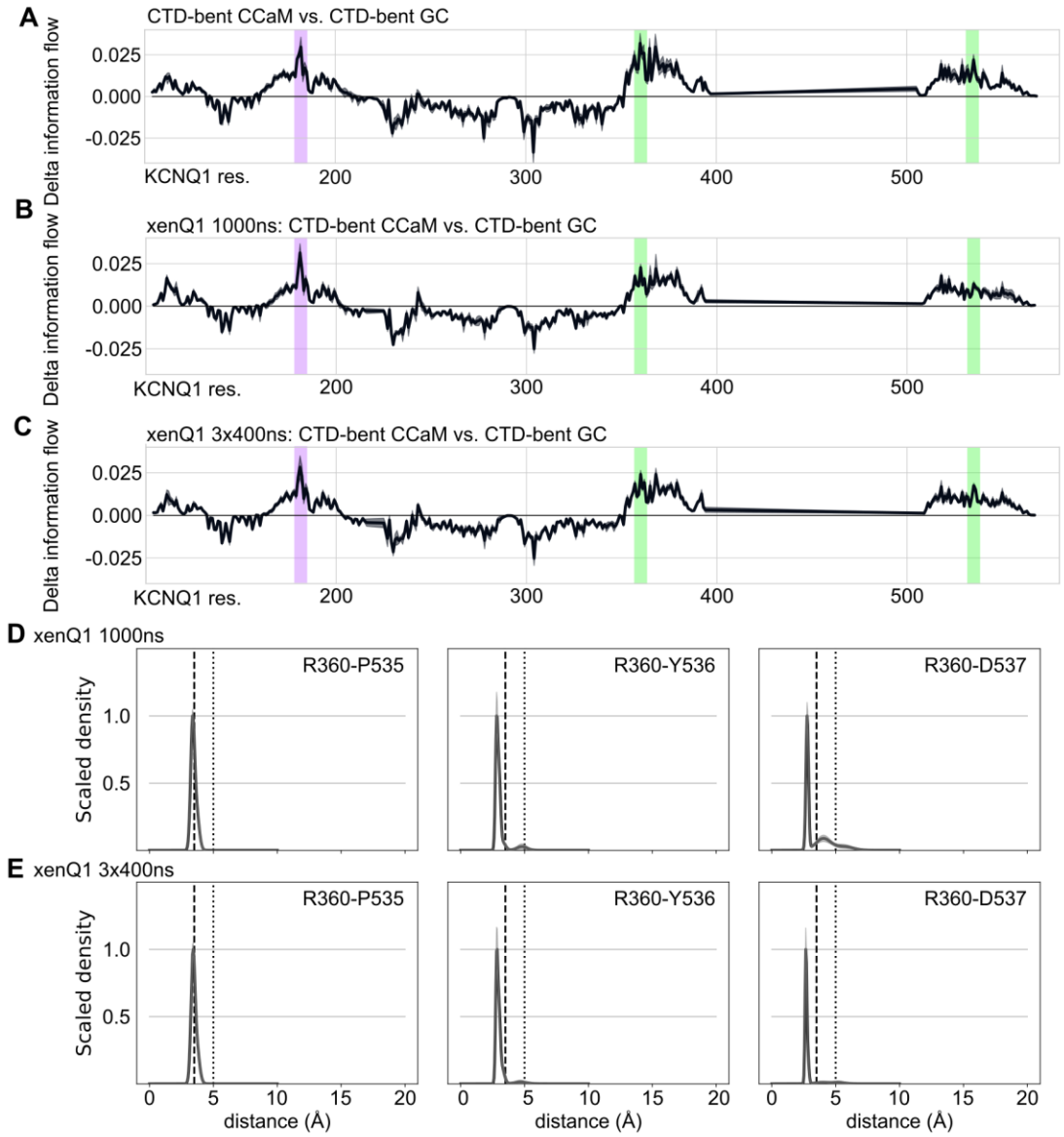

Supplementary Figure S9. Delta information flow plots and interactions at the CTD hub. Related to Main Figure 5. (A-C) Δinformation flow comparing the profiles using CaM C-lobe versus gating charges as source, of **(A)** human KCNQ1/CaM CTD-bent simulations, **(B)** *Xenopus* CaM/KCNQ1 1μs, and **(C)** 3x400ns simulations, respectively. **(D-E)** Scaled distance densities of selected interactions in the CTD hub of *Xenopus* KCNQ1/CaM CTD-bent simulations for 1μs **(D)** and 3x400ns **(E)**, respectively. Average, SEM and standard deviation are calculated over subunits.

Supplementary Figure S10.

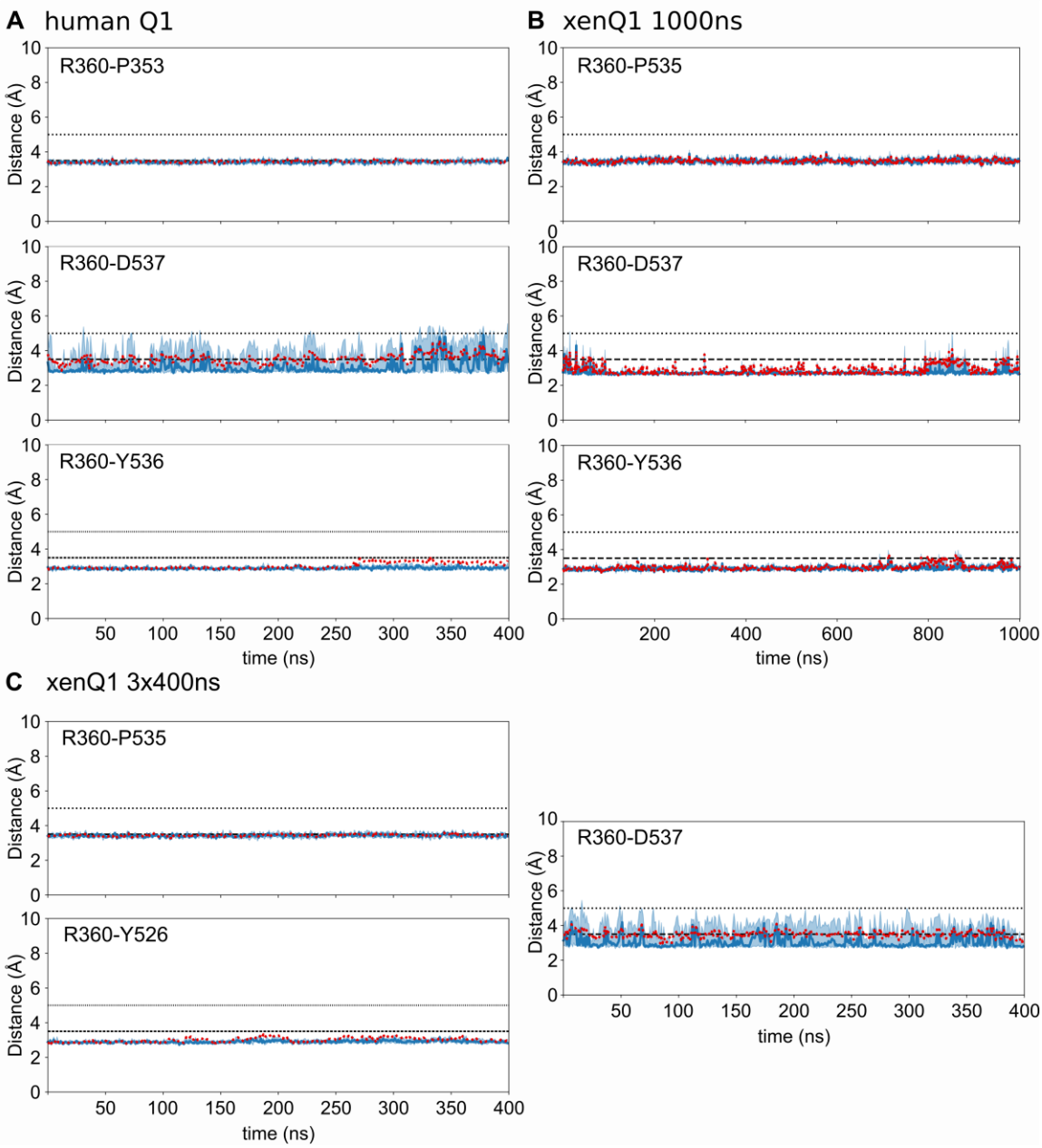

Supplementary Figure S10. Interaction distances between residues at the KCNQ1 CTD-hub. Related to Main Figure 5. (A-C) Time series of CTD-hub interaction distances from human KCNQ1/CaM CTD-bent simulations **(A)**, *Xenopus* CaM/KCNQ1 1μs **(B)**, and 3x400ns simulations **(C)**, respectively. The plots show the median (blue line), mean (red dots), as well as the 25th and 75th percentiles (shaded). Statistics are obtained from all subunit trajectories.

Supplementary Figure S11.

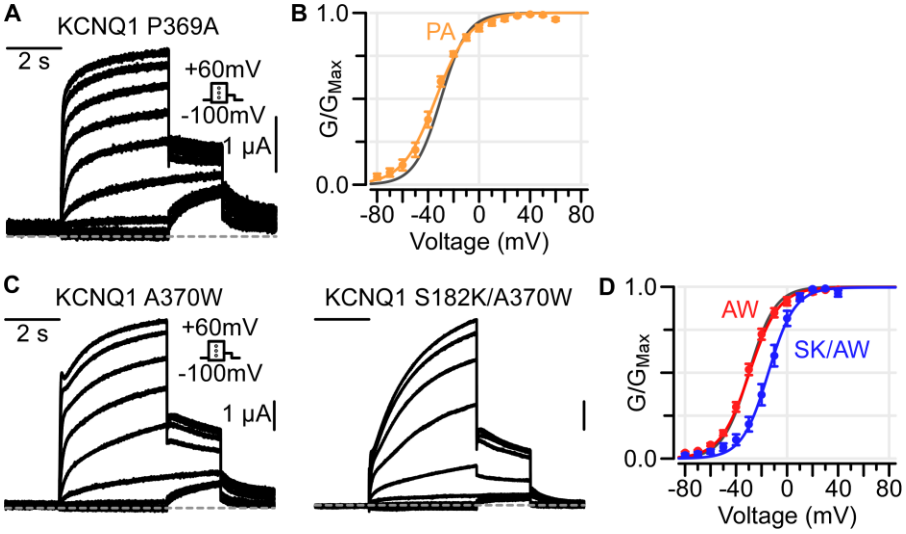

Supplementary Figure S11. Additional electrophysiology data on mutations in the KCNQ1 CTD. Related to Main Figure 6. (A-B) Exemplar KCNQ1 P369A currents and average G-V curve (orange curve, n = 7, $V_{1/2}$ = -33.3±1.43 mV). Grey GV curve is WT. **(C-D)** Exemplar KCNQ1 A370W (AW) and S182K/A370W (SK/AW) mutants. Average G-V curves are red for AW (n = 8, $V_{1/2}$ = -29.53±1.11 mV) and blue for SK/AW (n = 4, $V_{1/2}$ = -14.74±1.52 mV) mutants. Grey GV curve is WT.

Supplementary Table S1. Summary G-V relationship fits for mutagenesis scan of the KCNQ1 S2-S3 linker. Errors reported are SEM. 95% confidence intervals and p-values were computed by one-way ANOVA followed by Tukey's HSD test.

KCNQ1	V_s	$V_{1/2}$ (mV)	n	$\Delta V_{1/2}$ (mV)	$\Delta V_{1/2}$ 95% CI	p-value
WT	0.1±0.003	-30.01±0.64	18			
C180A	0.087±0.001	-17.76±0.48	5	12.25	[5.68,18.82]	1E-06
C180W	0.085±0.01	-28.22±0.94	5	1.79	[-4.78,8.36]	0.99998
R181A	0.094±0.004	-20.15±0.66	5	9.86	[3.29,16.43]	5.3E-05
R181W	0.079±0.007	-21.1±2.14	5	8.91	[2.34,15.48]	0.00049
R181Q	0.106±0.003	-27.8±1.04	7	2.21	[-3.58,8]	0.99762
R181E	0.122±0.006	-8.74±1.48	10	21.27	[16.15,26.4]	9.2E-07
S182A	0.091±0.002	-21.17±1.1	6	8.84	[2.72,14.97]	0.00013
S182W	0.085±0.004	-23.27±1.45	6	6.74	[0.62,12.87]	0.01575
S182D	0.085±0.005	-26.79±2.44	8	3.22	[-2.3,8.74]	0.84119
S182K	0.11±0.003	-11.51±0.87	13	18.50	[13.77,23.23]	9.2E-07
K183A	0.1±0.004	-19.04±1.02	5	10.98	[4.41,17.54]	4.1E-06
K183W	0.094±0.004	-22.94±1.28	7	7.070	[1.28,12.86]	0.00332
Y184W	0.103±0.003	-29.31±0.71	5	0.71	[-5.86,7.27]	1
V185A	0.117±0.002	-22.44±0.93	5	7.57	[1,14.14]	0.00822
V185W	0.088±0.008	-27.98±2.51	5	2.04	[-4.53,8.6]	0.99986
G186A	0.091±0.001	-25.6±1.6	5	4.41	[-2.16,10.98]	0.63288
G186W	0.081±0.005	-25.6±0.6	5	4.41	[-2.16,10.98]	0.63318
L187A	0.103±0.001	-30.11±1.22	4	-0.10	[-7.28,7.08]	1
L187W	0.094±0.007	-28.35±2.26	5	1.66	[-4.91,8.23]	0.99999

Supplementary Table S2. Summary G-V relationship fits for KCNQ1 WT channel co-expressed with CaM mutants. Errors reported are SEM. WT indicate co-expression with CaM WT. 95% confidence intervals and p-values were computed by one-way ANOVA followed by Tukey's HSD test.

CaM	V_s	$V_{1/2}$ (mV)	n	$\Delta V_{1/2}$ (mV)	$\Delta V_{1/2}$ 95% CI	p-value
WT	0.094±0.003	-29.11±0.62	12			
N98S	0.094±0.003	-25.73±0.63	7	3.38	[-0.84,7.6]	0.293
G99K	0.098±0.003	-27.4±1.2	5	1.71	[-3.01,6.44]	0.998
Y100A	0.11±0.002	-26.32±0.21	3	2.79	[-2.94,8.52]	0.956
Y100K	0.103±0.005	-29.67±0.67	4	-0.56	[-5.68,4.56]	1
Y100D	0.103±0.004	-22.21±0.5	9	6.90	[2.99,10.82]	1.95E-6
I101K	0.085±0.004	-30.18±1.54	3	-1.06	[-6.79,4.66]	1
I101E	0.087±0.002	-30.01±0.68	3	-0.90	[-6.63,4.82]	1
N138L	0.092±0.002	-19.58±0.46	5	9.53	[4.81,14.26]	8.217E-7
N138R	0.099±0.003	-22±0.9	5	7.11	[2.38,11.83]	6.867E-5
N138D	0.102±0.002	-24.1±0.68	6	5.02	[0.58,9.45]	0.0115
Y139A	0.086±0.002	-28.38±0.59	3	0.73	[-5,6.46]	1
Y139K	0.085±0.003	-28.34±1.4	3	0.77	[-4.96,6.5]	1
Y139E	0.084±0.001	-29.39±1.41	3	-0.28	[-6.01,5.45]	1
E140A	0.102±0.002	-25.02±1.24	13	4.095	[0.54,7.65]	0.00876
E140R	0.082±0.001	-27.49±0.98	8	1.62	[-2.43,5.67]	0.994
E140Q	0.092±0.002	-26.03±0.36	6	3.08	[-1.36,7.51]	0.554
E141K	0.086±0.002	-24.19±1.16	5	4.92	[0.19,9.64]	0.0323
F142L	0.09±0.006	-34.09±0.82	5	-4.98	[-0.84,7.6]	0.0127

Supplementary Table S3. Summary G-V and F-V relationship fits for experiments performed in Main Figure 4. Units for all $V_{1/2}$ are in mV. Errors reported are SEM.

	n	*G-V* V_s	*G-V* $V_{1/2}$
Q1*-psWT	10	0.09±0.003	-45.83±0.96
Q1*-S182K	10	0.081±0.001	-30.71±0.54
Q1-WT+E1	5	0.066±0.002	29.76±1.59
Q1-S182K+E1	7	0.05±0.001	52.80±3.40
Q1-S338F	6	0.07±0.003	-6.27±1.28
Q1-S338F/S182K	11	0.089±0.002	0.056±0.81

	n	F_1*-V* V_s	F_1*-V* $V_{1/2}$	F_2*-V* V_s	F_2*-V* $V_{1/2}$
Q1*-psWT	10	0.062±0.002	-42.00±1.16	0.05±0.005	69.27±5.1
Q1*-S182K	10	0.065±0.003	-38.87±0.72	0.044±0.003	63.66±4.00